Molecular dynamics simulations of carbon nanotubes in water

By J. H. Walther†, R. Jaffe‡, T. Halicioglu‡ AND P. Koumoutsakos†¶

We study the hydrophobic/hydrophilic behavior of carbon nanotubes using molecular dynamics simulations. The energetics of the carbon-water interface are mainly dispersive but in the present study augmented with a carbon quadrupole term acting on the charge sites of the water. The simulations indicate that this contribution is negligible in terms of modifying the structural properties of water at the interface.

Simulations of two carbon nanotubes in water display a wetting and drying of the interstice between the nanotubes depending on their initial spacing. Thus, initial tube spacings of 7 and 8 Å resulted in a drying of the interface whereas spacing of > 9 Å remain wet during the course of the simulation.

Finally, we present a novel particle-particle-particle-mesh algorithm for long range potentials which allows for general (curvilinear) meshes and "black-box" fast solvers by adopting an influence matrix technique.

1. Introduction

The unique mechanical and electrical properties of carbon nanotubes (see Odom *et al.* (2000)) have prompted an interest for technical application in a number of fields including biosensors (Balavoine *et al.* (1999)), atomic force microscopy (Jarvis *et al.* (2000); Moloni *et al.* (1999); Li *et al.* (1999)), and fuel storage (Wang & Johnson (1999); Rzepka *et al.* (1998); Gordon & Saeger (1999); Lee & Lee (2000)). A key aspect of these applications is the interaction of the surrounding fluid with the carbon nanotube and, in particular, the hydrophobic/hydrophilic behavior of carbon nanotubes.

The graphite-water interface is known to be strongly hydrophobic (e.g. Müller *et al.* (1996)) and to exhibit a preferred orientation of the water dipole moment parallel to the interface (Ulberg & Gubbins (1995), Allen *et al.* (1999), and Shevade *et al.* (1999)). Most of the studies on graphite-water systems have involved planar interfaces or idealized geometries (Wallqvist & Berne (1995)). The presence of an electrostatic quadrupole moment interaction between graphite and water as proposed by Vernov & Steele (1992) and subsequently measured by Whitehouse & Buckingham (1993) has mostly been neglected in the previous studies. Marković *et al.* (1999, 2000) included the quadrupole interaction in their numerical study of water scattering from a graphite surface, but did not provide information of the importance of this term. Thus, to study the structural properties of water surrounding a carbon nanotube, we perform detailed molecular dynamics simulations of a 12.52 Å diameter carbon nanotube with chirality $(16, 0)$ in water (see Fig. 1) using Morse harmonic bond potentials and Lennard-Jones potentials to model the carbon nanotube and the flexible model for water by Teleman *et al.* (1987). We include

† Inst. of Computational Sciences, ETH Zürich, Switzerland
‡ NASA Ames Research Center, USA
¶ also at Center for Turbulence Research, NASA Ames/Stanford Univ.

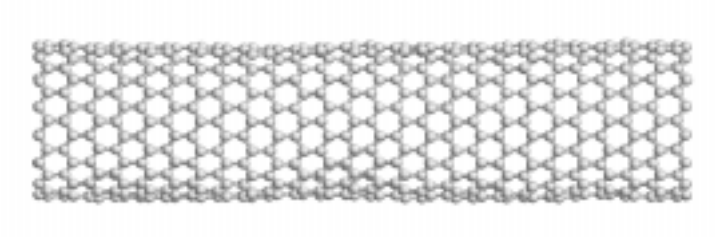

FIGURE 1. Sketch of the carbon nanotube.

and compare the effect of the electrostatic quadrupole as suggested in Vernov & Steele (1992).

Another important issue related to the carbon-water interface is the wetting and drying of the interstices in a bundle of carbon nanotubes. The drying can lead to hydrophobic aggregation of the tubes (Lum *et al.* (1999)), changing the mechanical and electrostatic properties of the system. Thus, in the second part of the study, we consider two carbon nanotubes in water initially aligned and with an initial spacing S_0 between the carbon nanotube walls.

2. Governing equations and solution procedure

The carbon nanotube-water system is modeled using classical molecular dynamics simulations in the micro canonical (NVE) ensemble. The governing Newton's equations are integrated in time using the leap frog scheme (Allen & Tildesley (1987)) subject to periodic boundary conditions.

The water is described by the flexible (TJE) water model of Teleman *et al.* (1987) featuring harmonic bonds between the oxygen and hydrogen sites, which also holds the partial charges.

The restrictions imposed on the time integrator by the eigen-frequency of water of the order of $3500\,\mathrm{cm}^{-1}$ (Dang & Pettitt (1987)) are not too severe since the highest eigen-frequency of the carbon nanotube is of the order of $1500\,\mathrm{cm}^{-1}$ (Saito *et al.* (1998)). Thus, a time step of $\delta t = 0.2\,\mathrm{fs}$ proved sufficient for stability and conservation of energy and has been used throughout.

2.1. *Potentials*

2.1.1. *Carbon nanotube*

The carbon nanotube is modeled by a Morse bond, a harmonic cosine angle, and a 2-fold torsion potential as

$$U(r_{ij},\theta_{ijk},\phi_{ijkl}) = K_{Cr}(\xi_{ij}-1)^2 + \frac{1}{2}K_{C\theta}(\cos\theta_{ijk}-\cos\theta_C)^2 + \frac{1}{2}K_{C\phi}\left(1-\cos 2\phi_{ijkl}\right), \tag{2.1}$$

where

$$\xi_{ij} = e^{-\gamma(r_{ij}-r_C)}, \tag{2.2}$$

and θ_{ijk} and ϕ_{ijkl} represent all the possible bending and torsion angles, and r_{ij} represents all the distances between bonded atoms. K_C, $K_{C\theta}$, and $K_{C\phi}$ are the force constants of the bond, angle, and torsion potentials, respectively, and r_C, θ_C, and ϕ_C are the corresponding reference geometry parameters for graphene. The Morse and angle parameters given by Guo *et al.* (1991) and Tuzun *et al.* (1996) are listed in Table 1.

K_{Cr}	=	$478.9\,\mathrm{kJ\,mol^{-1}\,\AA^2}$	r_C	=	$1.418\,\mathrm{\AA}$
$K_{C\theta}$	=	$562.2\,\mathrm{kJ\,mol^{-1}}$	θ_C	=	120.00°
$K_{C\phi}$	=	$25.12\,\mathrm{kJ\,mol^{-1}}$	γ	=	$2.1867\,\mathrm{\AA^{-1}}$
ϵ_{CC}	=	$0.4396\,\mathrm{kJ\,mol^{-1}}$	σ_{CC}	=	$3.851\,\mathrm{\AA}$

TABLE 1. Parameters for the carbon interaction potentials (Tuzun *et al.* (1996) and Rappé *et al.* (1992)). K_{Cr}, r_C, and γ are the parameters for the Morse potential, $K_{C\theta}$ and θ_C are the angle parameters, and $K_{C\phi}$ is the torsion parameter. ϵ_{CC} and σ_{CC} are the Lennard-Jones parameters for the carbon-carbon interaction.

The Morse bond and angle terms maintain the C-C bond length and hexagonal ring structure of the carbon nanotube, and the torsion term is needed to provide a measure of the strain due to curvature of the reference graphene sheet. This curvature strain prevents collapse of the nanotobe and imparts stiffness with respect to bending deformations. To obtain a physically reasonable torsion parameter, quantum chemistry calculations were carried out for planar and curved tetracene ($C_{18}H_{12}$), which consists of 4 hexagonal rings fused together in a strip-like part of the circumference of a zigzag carbon nanotube. The calculations were carried out using the Gaussian98 software package (Frisch *et al.* (1998)). Tetracene is planar with a $9.778\,\mathrm{\AA}$ separation between the C-C bonds on opposite ends of the molecule. If the tetracene molecule were extracted from a $(16, 0)$ nanotube and held rigid such that end-to-end separation would be $8.795\,\mathrm{\AA}$. Quantum chemistry calculations were carried out using density functional theory (DFT) with the hybrid nonlocal B3LYP functional (Becke (1993)) as implemented in the Gaussian98 software package. For each amount of curvature, the molecular geometry was completely optimized except for the end-to-end distance constraint. The energy difference between the curved and planar tetracene molecules (ΔE_{curv}) was determined to be $71.11\,\mathrm{kJ\,mol^{-1}}$using the standard 6-31G(d) contracted Gaussian atomic orbital basis set. The curvatures considered were appropriate for $(n, 0)$ nanotubes with $n = 12, 24$. The torsion parameter $K_{C\phi}$ was determined from

$$K_{C\phi} = 2\Delta E_{curv} \left(\sum_i^{84} 1 - \cos 2\phi_i \right)^{-1}, \tag{2.3}$$

with the summation over the complete set of 84 torsion angles in the optimized curved tetracene molecule (4 for each C-C bond). For all cases studied, $K_{C\phi}$ was between 24.60 and $25.25\,\mathrm{kJ\,mol^{-1}}$. The value of $25.12\,\mathrm{kJ\,mol^{-1}}$was selected for the present study.

A Lennard-Jones term is furthermore added to account for the steric and van der Waals carbon-carbon interaction

$$U(r_{ij}) = 4\epsilon_{CC} \left[\left(\frac{\sigma_{CC}}{r_{ij}} \right)^{12} - \left(\frac{\sigma_{CC}}{r_{ij}} \right)^{6} \right]. \tag{2.4}$$

where ϵ_{CC} and σ_{CC} are obtained from the UFF force field (Rappé *et al.* (1992)), see Table 1.

The bond potentials can be efficiently computed on scalar and vector architectures, in the latter case by rearranging the list of carbon bonds to secure vectorization. The non-bond Lennard-Jones potential is computed using a standard cell index table and spherical truncation.

K_{Wr}	=	$4637\,\mathrm{kJ\,mol^{-1}\,\AA^2}$	r_W	=	$1.0\,\mathrm{\AA}$
$K_{W\theta}$	=	$383\,\mathrm{kJ\,mol^{-1}rad^2}$	θ_W	=	109.47°
ϵ_{OO}	=	$0.65017\,\mathrm{kJ\,mol^{-1}}$	σ_{OO}	=	$3.166\,\mathrm{\AA}$
q_O	=	$-0.82\,\mathrm{e}$	q_H	=	$0.41\,\mathrm{e}$

TABLE 2. Parameters for the flexible (TJE) water model (Teleman *et al.* (1987)).

2.1.2. *Water model*

The flexible water model is described by harmonic bonds between the hydrogen-oxygen sites as

$$U(r_{ij},\theta_{ijk}) = \frac{1}{2}K_{Wr}(r_{ij}-r_W)^2 + \frac{1}{2}K_{W\theta}(\theta_{ijk}-\theta_W)^2, \tag{2.5}$$

where K_{Wr} and $K_{W\theta}$ are the parameters of the potential and $r_W = 1.0\,\mathrm{\AA}$ the reference bond length and angle $\theta_W = 109.47^\circ$ in (Teleman *et al.* (1987)).

Non-bonded interactions between the water molecules involve a Lennard-Jones term between the oxygen atoms

$$U(r_{ij}) = 4\epsilon_{OO}\left[\left(\frac{\sigma_{OO}}{r_{ij}}\right)^{12} - \left(\frac{\sigma_{OO}}{r_{ij}}\right)^{6}\right], \tag{2.6}$$

and a Coulomb potential

$$U(r_{ij}) = \frac{1}{4\pi\epsilon_0}\frac{q_i q_j}{r_{ij}}, \tag{2.7}$$

where ϵ_0 is the permittivity in vacuum, and q_i is the partial charge, $q_O = -0.82$ and $q_H = 0.41$, respectively (Teleman *et al.* (1987)). The Coulomb interaction is computed using a smooth truncation as

$$U(r_{ij}) = \frac{1}{4\pi\epsilon_0}\left(\frac{q_i q_j}{r_{ij}} - E_s(r_{ij})\right), \tag{2.8}$$

where $E_s(r_{ij})$ is a smoothing function

$$E_s(r_{ij}) = \frac{q_i q_j}{r_c} - (r_{ij}-r_c)\frac{q_i q_j}{r_c^2}, \tag{2.9}$$

and r_c the radius of truncation (Levitt *et al.* (1997)). The truncation of the Coulomb potential has been shown to have little effect on the thermodynamic and structural properties of water for cutoffs larger than 6 Å (Andrea *et al.* (1984)), and in this study we employ a value of 9.50 Å ($3\sigma_{OO}$) The parameters of the potential are summarized in Table 2.

Alternatively, the Coulomb potential can be computed without truncation using the P^3M algorithm as described in Section 4.

2.1.3. *Carbon-water interaction*

The carbon-water interaction consists of a Lennard-Jones term between the carbon and oxygen sites

$$U(r_{ij}) = 4\epsilon_{CO}\left[\left(\frac{\sigma_{CO}}{r_{ij}}\right)^{12} - \left(\frac{\sigma_{CO}}{r_{ij}}\right)^{6}\right], \tag{2.10}$$

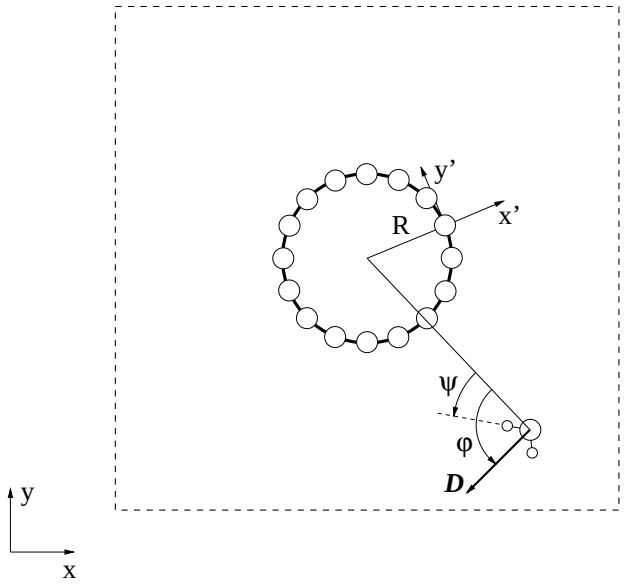

FIGURE 2. Sketch of the carbon nanotube-water system. R is the radius of the carbon nanotube, and $\boldsymbol{D}$ the water dipole moment. (x', y') is the local co-ordinate system used in the calculation of the quadrupole interactions. The orientation of the water molecules is given in terms of the angles φ and ψ. The dashed box indicates the position of the periodic boundary.

where parameters of the potential ϵ_{CO} and σ_{CO} are obtained from Vernov & Steele (1992), and a quadrupole interaction between the carbon atoms and the partial charges on the water hydrogen and oxygen atoms

$$U(\boldsymbol{r}_\alpha, \boldsymbol{r}_\beta) = \frac{1}{3}\frac{q}{4\pi\epsilon_0}\sum_{\alpha,\beta}\Theta_{\alpha,\beta}\frac{3r_\alpha r_\beta - r^2\delta_{\alpha\beta}}{r^5}, \tag{2.11}$$

where α, β run over all Cartesian co-ordinates x, y, z, and r is the distance between the charge site and the quadrupole carbon site. $\delta_{\alpha\beta}$ is the delta function, and $\Theta_{\alpha,\beta}$ is the quadrupole moment tensor (Hansen & Bruch (1995)).

In the present study, we evaluate Eq. (2.11) in a local co-ordinate system (x', y', z') centered at the quadrupole site, see Fig. 2. If x' is the wall normal direction we have

$$\Theta_{xx} = -2\Theta_{yy} = -2\Theta_{zz}, \tag{2.12}$$

with all other components equal to zero (see Hansen & Bruch (1995)). The quadrupole interaction is truncated at $r = r_c$, where r_c is the cutoff radius of the Lennard-Jones and Coulomb potentials. Note that the effect of the quadrupole moment is an attraction of positive charge (hydrogen) towards the nanotube wall and conversely a repulsion of negative charge (oxygen). The parameters for the carbon-water potentials are summarized in Table 3.

2.2. *Simulation details*

The water molecules are initially placed on a regular lattice, and the system is equilibrated to obtain the desired temperature and bulk density of the water. The equilibration is divided into two parts for the cases involving two carbon nanotubes. In the first part, the nanotubes are held at a fixed position ("frozen") in order to allow the water molecules

$$\epsilon_{CO} = 0.3126\,\mathrm{kJ\,mol^{-1}} \quad \sigma_{CO} = 3.19\,\text{Å} \quad \Theta_{\alpha,\beta} = 3.03\times10^{-40}\,\mathrm{Cm^2}$$

TABLE 3. Parameters for the carbon-water interaction potentials, (see Vernov & Steele (1992) and Whitehouse & Buckingham (1993)).

to "settle" between the tubes. The carbon nanotubes are released in the second part of the equilibration which involves thermal equilibration and are free to move during the remainder of the simulation. The temperature control is performed by scaling the velocity of the atoms every 500 time steps (every 0.1 ps) and is switched off after the equilibration at 4 ps.

The volume of the computational box is adjusted to match the target density of water in the far-field. The regulation of the volume is performed by re-positioning the periodic boundary in the $x-y$ plane (see Fig. 2) while keeping the extent of the box in the z-direction fixed. This procedure prevents any deformation of the carbon nanotube during the volume adjustment.

3. Results

The molecular dynamics simulations involve single and a pair of carbon nanotubes in water at a temperature of 300 K and a bulk water density of $\rho_0 = 997\,\mathrm{kg\,m^{-3}}$. The carbon nanotube is a $(16,0)$ nanotube with a radius (R) in vacuum of 6.26 Å, and the length of the computational box (L) is $8.6R$ (53.8 Å).

The results are presented in terms of radial density and probability density profiles of the orientation of the water dipole moment ($P(\cos\varphi)$) and the orientation of the OH bonds ($P(\cos\psi)$) (see Fig. 2) where

$$P(\cos\varphi) = \frac{<\cos\varphi>_r +1}{2}, \qquad P(\cos\psi) = \frac{<\cos\psi>_r +1}{2}, \tag{3.1}$$

and $<\ldots>_r$ denotes the average value at the position r. Notice that $\cos\varphi = +1$ indicates a direction along the outward surface normal, $\cos\varphi = 0$ a direction parallel to the normal, and $\cos\varphi = -1$ a direction in the negative surface normal. The profiles are sampled every 20 fs in 30 bins of constant volume extending from the surface of the nanotube.

Studies of bulk water and water with a free surface (slab) are provided as a reference. The average potential energies of the bulk are found in good agreement with previous studies using the same TJE water model by Teleman *et al.* (1987) (TJE), Wallqvist & Teleman (1991) (WT), and Mizan *et al.* (1994) (MSZ), see Table 4.

3.1. *Single carbon nanotube*

To study the influence of the quadrupole moment on the structural properties of water at the carbon-water interface, we have conducted simulations of one carbon nanotube in water. The nanotube consists of 832 carbon atoms and the water consists of 2088 water molecules. The system is equilibrated until the energetics settle around 4 ps, and the statistics are collected every 20 fs until $t = 40$ ps, a total of 1800 samples. The numerical parameters are summarized in Table 5.

The simulations of both one and two carbon nanotubes in water revealed damped oscillations of the potential energy of the carbon-carbon Lennard-Jones interaction with

		TJE	WT	MSZ	present work
Bond length	(Å)	1.016	1.017	1.016	1.017
Bond angle	(degree)	104.9	104.9	104.9	104.9
Dipole	(D)	2.43	2.44	2.43	2.44
$U_{\rm inter}$	(kJ mol^{-1})	-45.3	-47.5	-47.3	-48.2
$U_{\rm intra}$	(kJ mol^{-1})	5.1	6.3	6.3	6.2
$U_{\rm pot}$	(kJ mol^{-1})	40.1	-40.7	-41.0	-41.9

TABLE 4. Comparison of present bulk properties with the results of Teleman *et al.* (1987) (TJE), Wallqvist & Teleman (1991) (WT), and Mizan *et al.* (1994) (MSZ).

Case	QP	N_W	N_C	t_m(ps)	type
1	no	2088	832	39	SCN
2	yes	2088	832	39	SCN
3	–	729	0	62	bulk
4	–	729	0		slab
5	–	–	832	39	vacuum

TABLE 5. Simulation cases for a single carbon nanotube (SCN), bulk and slab simulations, and a carbon nanotubes in vacuum. N_W is the number of water molecules, N_C is the number of carbon atoms, and t_m is the total simulation time.

a frequency in the range of 200 cm^{-1}. A separate simulation of one carbon nanotube in vacuum was prepared to estimate the eigen-frequencies of the tube, in particular the breathing frequency A_g (the first radial mode) of the tube. Monitoring the potential energy of the carbon-carbon Lennard-Jones interaction revealed a frequency of 173 cm^{-1} in good agreement with the theoretical value of 180 cm^{-1} (Saito *et al.* (1998)). The correlation between the carbon-carbon Lennard-Jones energy and the motion of the tube was verified in a separate simulation in vacuum in which radial oscillations where specifically imposed (not shown).

The radial density profiles of hydrogen and oxygen are shown in FIg. 3a and 3b for the cases excluding and including the quadrupole moment. The maxima of the oxygen and hydrogen profiles nearly coincide near the interface, indicating that the plane of the water molecules is parallel to the interface. These profiles are markedly different from those of the liquid-vapor interface (see Fig. 4), exhibiting a characteristic layering and a presence of hydrogen atoms beyond the extent of the oxygen atoms (at $r/R < 1.4$).

The density profiles are, in general, in good agreement with the study of Wallqvist (1990) for polarizable water in contact with a smooth wall and with grand canonical Monte Carlo simulations of water adsorption in graphite pores by Ulberg & Gubbins (1995).

The orientation of the water molecules at the carbon-water interface is inferred from the orientation of the water dipole moment as shown in Fig. 5. The water molecules in the closest proximity of the nanotube ($r/R = 1.47 - 1.55$) display a small inclination of $\approx 4^\circ$ towards the nanotube and turn to 74° (an inclination of 16° towards the bulk) at the point of minimum density ($r/R = 1.71 - 1.78$). The bulk properties are reached at

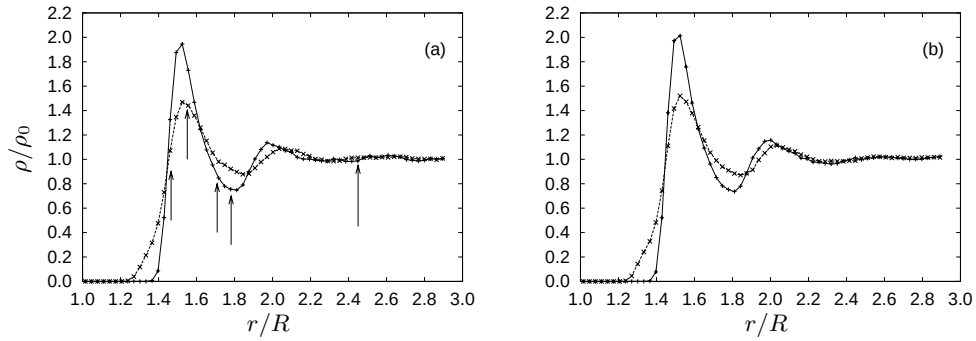

FIGURE 3. Water radial density profile. The arrows indicate the location of the bins used in the dipole orientation. (a) excluding the quadrupole moment; (b) including the quadrupole moment. –+–: oxygen density profile; –×–: hydrogen density profile.

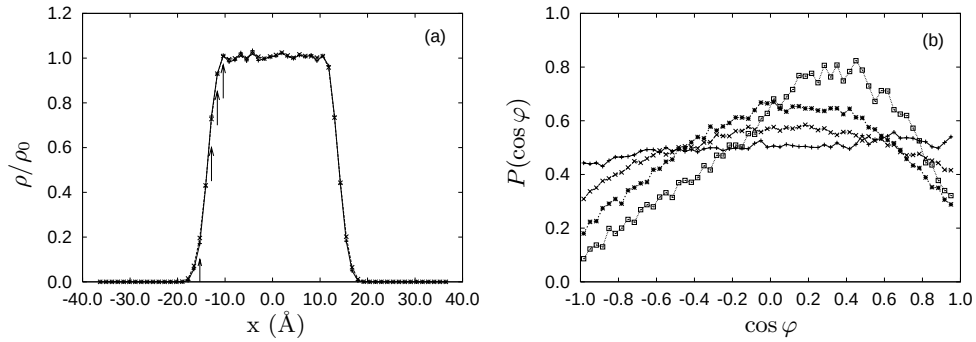

FIGURE 4. Density profile (a) and orientation of the water dipole moment (b) for a slab of water. The arrows in (a) indicate the the positions of the bin shown in (b): –+–: $x = -15.31$ Å; –×–: $x = -12.85$ Å; –∗–: $x = -11.62$ Å; –□–: $x = -10.39$ Å.

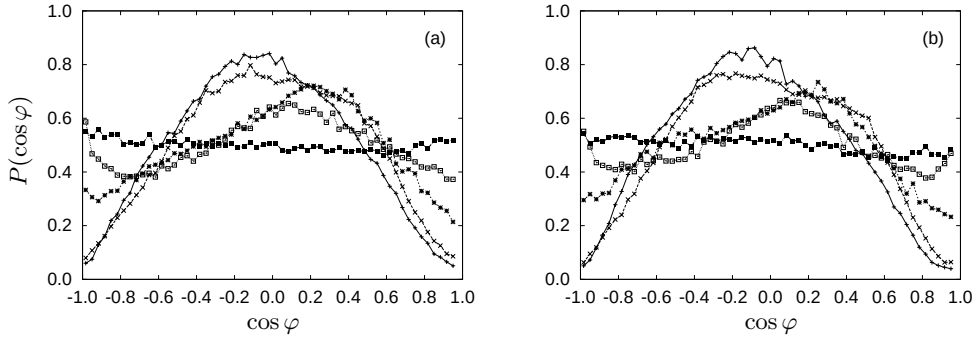

FIGURE 5. Dipole orientation at different distances from the carbon nanotube wall. (a) without the quadrupole moment; (b) with the quadrupole moment. –+–: $r/R = 1.47$; –×–: $r/R = 1.55$; –∗–: $r/R = 1.71$; –□–: $r/R = 1.78$; –■– : $r/R = 2.45$.

$r/R \geq 2.4$. These results are in good agreement with the work of Wallqvist (1990) and with the study of (ST2) water between hydrophobic surfaces by Lee *et al.* (1984).

Finally, we consider the orientation of the OH bonds as shown in Fig. 6. At $r/R = 1.47$ the OH bonds are directed towards the nanotube with an angle of $\approx 4°$, indicating that

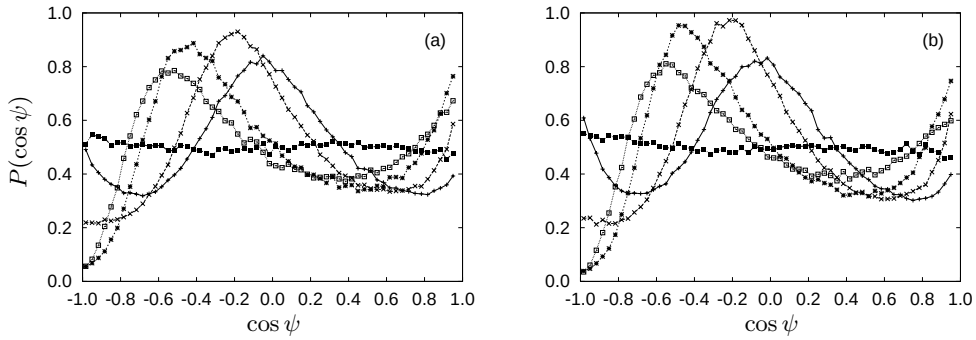

FIGURE 6. Orientation of the OH bonds at different distances from the carbon nanotube wall. (a) without the quadrupole moment; (b) with the quadrupole moment. –+– : $r/R = 1.47$; –×– : $r/R = 1.55$; –∗– : $r/R = 1.71$; –□– : $r/R = 1.78$; –■– : $r/R = 2.45$.

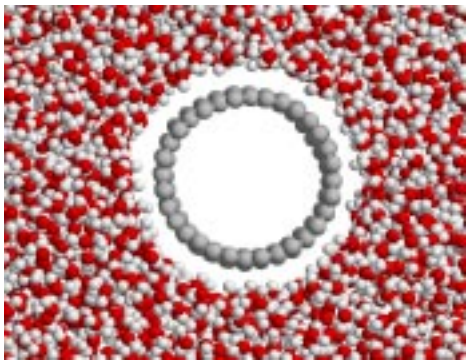

FIGURE 7. Snapshot of the atoms for the simulation of a single carbon nanotube in water. The interaction potentials include an electrostatic quadrupole moment (case 2).

the HOH plane is nearly parallel to the interface. A bimodal profile is observed for $r/R \leq 1.55$ with a high probability at 101°, 117°, and 123° for $r/R = 1, 71$, 1.78, and 2.45, respectively. From these structural properties of water, we conclude that the effect of the quadrupole moment on the density and dipole moment profiles is clearly small, but it appears to increase the probability of the extrema of the OH orientation. However, since the contribution from the quadrupole moment to the total carbon-water energetics is of the order of 0.1 %, further studies are being conducted to confirm these findings. A snapshot from the simulation including the quadrupole moment (case 2) is shown in Fig. 7. One can see a large number of hydro atoms on the nanotube side of the interfacial layer

3.2. *Twin carbon nanotubes*

The second part of the study involves two carbon nanotube in water, with each tube consisting of 832 atoms and a total of 4536 water molecules present. Four simulations have been performed, including three different initial tube spacings ($S_0 = 7$, 8, and 9 Å), and a sensitivity study has been conducted to determine the influence of the equilibration procedure. The number of water molecules and their initial positions are identical for each simulation, and only the initial spacing of the nanotubes is varied. The simulations are performed in the canonical ensemble, heating the system every 500 time steps (every

(a) 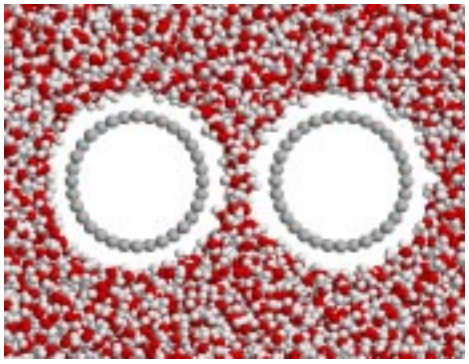 (b) 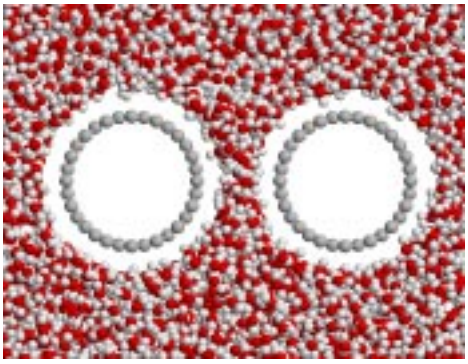

FIGURE 8. Snapshots of the water molecules after equilibration at 2 ps. (a): initial tube spacing of 7 Å (case 6); (b): initial tube spacing of 8 Å (case 7).

Case	$t_f/\delta t$	$t_h/\delta t$	S_0(Å)	N_W	N_C
6	10000	500	7.0	4536	1664
7	10000	500	8.0	4536	1664
8	10000	500	9.0	4536	1664
9	50000	500	7.0	4536	1664

TABLE 6. Simulation cases for a two carbon nanotubes. δt is the time step size, t_f the "freezing" time of the carbon nanotubes, $1/t_h$ the heating frequency, S_0 the initial distance between the nanotube walls, N_W the number of water molecules, and N_C the number of carbon atoms.

0.1 ps), but simulations in the micro canonical ensemble gave similar results (not shown). The equilibrated systems are shown in Fig. 8 for the two cases with an initial spacing of 7 Å and 8 Å, respectively. The numerical parameters are listed in Table 6.

The time history of the separation $S(t)$ between the carbon nanotubes is shown in Fig. 9 for the four cases. The simulation involving an initial tube spacing of 7 Å exhibits a decrease in spacing when the tubes are "released" after 10,000 time steps (2 ps). The spacing reaches a plateau of 5.8 Å at 4 ps but continues to decrease after 10 ps and reaches an equilibrium spacing of 3.49 ± 0.06 Å at 17 ps. This "drying" of the interface is in agreement with the studies on stacked plates by Wallqvist & Berne (1995), who showed that stable configurations of water in a hydrophobic environment requires the presence of two or more layers of water. Indeed, the level of the plateau coincides with the thickness of one layer of water $\approx 2\sigma_{OO} = 6.3$ Å. The position of the atoms during the drying is shown in Fig. 10.

An additional simulation was conducted to study the effect of the duration of the initial "freezing" of the nanotube. The equilibration was extended to 10 ps (case 9), but with a persistent drying of the interface cf. Fig. 9.

A similar time history is observed for the nanotube starting from an initial spacing of 8 Å. The plateau is reached after 7 ps, and the tube spacing decreases rapidly after 9–10 ps to reach the equilibrium distance after 12 ps.

Finally, the nanotubes placed with an initial spacing of 9 Å (case 8) remain wetted during the simulation cf. Fig. 9. This spacing is consistent with the thickness of two water layers of $9.2 - 10.2$ Å depending on the staggering of the carbon-oxygen system.

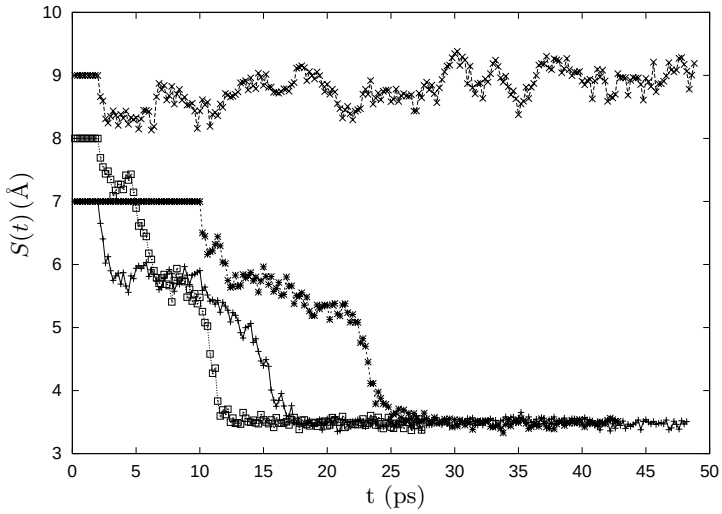

FIGURE 9. Time history of the spacing between two carbon nanotubes in water. –+–: Case 6; –□–: Case 7; –x–: Case 8; –∗–: Case 9.

4. P^{3}M algorithm

The smooth truncation of long range potentials (eg. the Coulomb potential) is a viable approach for homogeneous systems ie. where the system is locally neutral $\sum_i q_i = 0$ (where q_i is the "generalized charge" or the strength of the particle). In molecular dynamics simulations neutral systems are often assumed, whereas such an assumption is invalid in astrophysics (where q_i corresponds to mass) and in fluid dynamics (where q_i corresponds to circulation or vorticity). For these problems and for simulations requiring higher accuracy than warranted by the smooth truncation, the Particle-Particle-Particle-Mesh algorithm (P^{3}M) is an efficient alternative. The algorithm gains it efficiency by employing fast Fourier transforms on a regular mesh for the solution of the Poisson equation for the electrostatic potential (Φ)

$$\nabla^2 \Phi = -\frac{\rho}{\epsilon_0}, \tag{4.1}$$

where ρ is the charge density and its accuracy by a local particle-particle correction to resolve any sub-grid scales not properly resolved by Eq. (4.1). Sub-grid scale are present if the projected charge density is a smooth approximation to the true charge density, which is normally the case in molecular dynamics simulation, but not the case in particle (vortex) methods. The original method by Hockney & Eastwood (1988) proceeds as follows:

- Project the particle charge onto the mesh to obtain the charge density (ρ).
- Solve Eq. (4.1) for the electrostatic potential (Φ).
- Compute the electrostatic field on the mesh as $\boldsymbol{E} = -\boldsymbol{\nabla}\phi$.
- Project the electrostatic field onto the particles and compute the resolved particle force as: $\tilde{\boldsymbol{f}}_i = q_i \boldsymbol{E}(\boldsymbol{x}_i)$.
- Compute the sub-grid scale forces as a local particle-particle correction, $\boldsymbol{C}(r_{ij})$.
- The total particle force is $\boldsymbol{f}_p = \tilde{\boldsymbol{f}}_p + \boldsymbol{C}$, where $\boldsymbol{C}$ is the total sub-grid force.

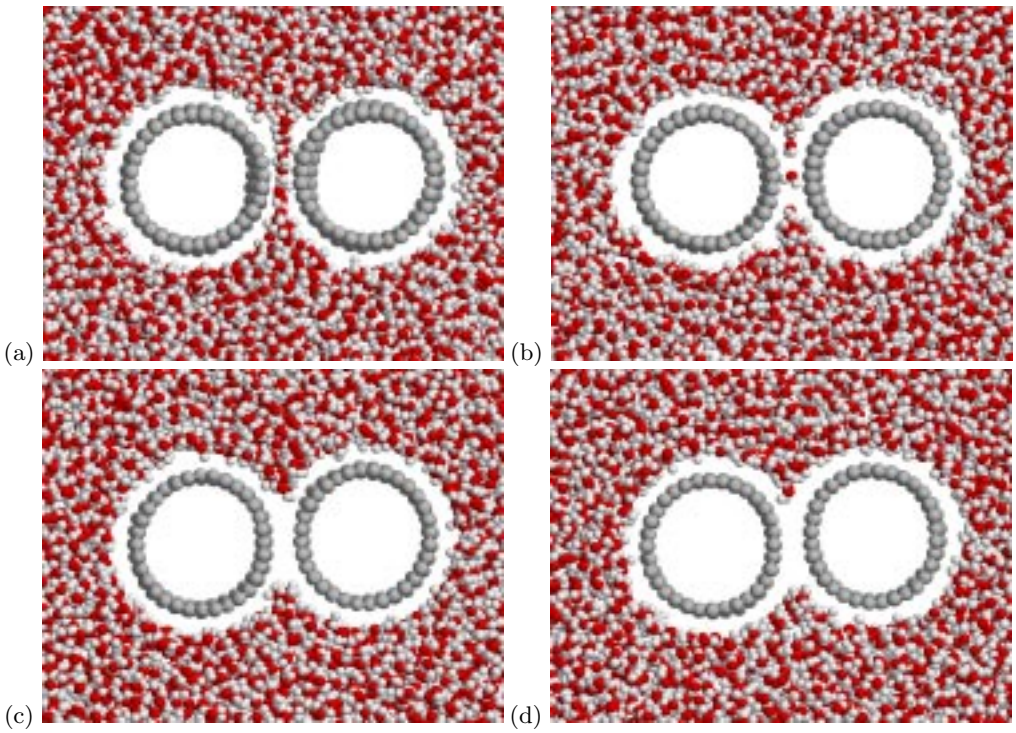

FIGURE 10. Snapshot of the water molecules during the drying process for case 7 at $t = 12$, 14, 16, and 18, ps (a-d), respectively.

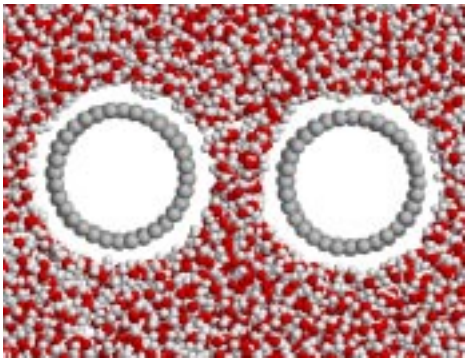

FIGURE 11. Snapshot of the water molecules during wetting (case 8) at $t = 18$ ps.

The success of the Hockney & Eastwood (1988) algorithm is based on an inversion of the Poisson equation

$$\Phi(\boldsymbol{x}) = \int G(\boldsymbol{x} - \boldsymbol{y}) * \rho \, \mathrm{d}\boldsymbol{y}, \tag{4.2}$$

where G is the Green's function to ∇^2. The convolution (4.2) is computed in Fourier space employing an "optimized" Green's function ($\hat{\Phi} = \hat{G}_{opt} * \hat{\rho}$) to secure a prescribed and isotropic sub-grid scale ie. $\boldsymbol{C}(\boldsymbol{x}_i - \boldsymbol{x}_j) = \boldsymbol{C}(r_{ij})$, where $r_{ij} = |\boldsymbol{x}_i - \boldsymbol{x}_j|$.

An alternative P^3M algorithm proposed by Theuns (1994) estimates the resolved (anisotropic) electrostatic potential from the projected charge density by computing the

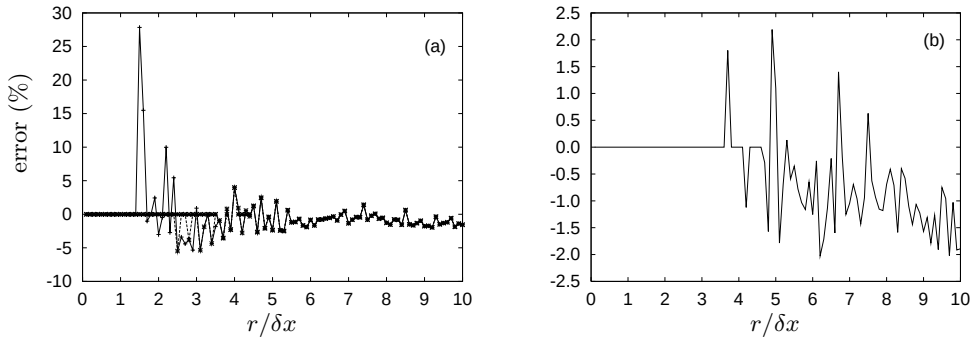

FIGURE 12. Comparison between the P^{3}M forces and the exact force for two particles in a periodic domain. The different curves in (a) demonstrate the effect of the cutoff radius (r_c) of the particle-particle correction. –+–: $r_c/h = 1$; –x–: $r_c/h = 2$; –□–: $r_c/h = 3$. (b) shows the error on a test particle displaced from a group of 10^4 particles centered in the computational domain.

convolution in real space as

$$\tilde{\boldsymbol{E}}(\boldsymbol{x}_j) \approx \frac{h^3}{4\pi\epsilon_0} \sum_i^M \rho_i \frac{\boldsymbol{x}_i - \boldsymbol{x}_j}{|\boldsymbol{x}_i - \boldsymbol{x}_j|^3}, \tag{4.3}$$

where h is the mesh spacing and M is the number of mesh points involved in the project step. The algorithm proceeds by subtracting this estimate for the resolved field for particles in close proximity, and the corresponding local particle-particle correction is the exact $1/r$ relation.

The present algorithm replaces the approximate convolution in real space (4.3) by an influence matrix technique as

$$\mathcal{E}_i^h = \mathcal{M}_{ij}^h \mathcal{R}_j^h, \tag{4.4}$$

where $\mathcal{M}_{ij}^h$ is the influence matrix describing the electrostatic field $\mathcal{E}_i^h$ at the i-th grid point as induced by the charge density $\mathcal{R}_j^h$ at the j-th grid point. The size of the vectors $\mathcal{E}_i^h$ and $\mathcal{R}_j^h$ is governed by the number of mesh points involved in the projection and the number of nearest grid points included in the particle-particle correction. The algorithm is described in more detail in (Walther & Koumoutsakos (2000)).

To demonstrate the accuracy of the present P^{3}M algorithm, we consider the electrostatic force between two charged particles in a periodic domain and study the errors for different particle spacings and for different cutoff distances (r_c) for the particle-particle correction. The difference between the P^{3}M force and the value compute by direct summation over a large number of images is shown in Fig. 12a. The present P^{3}M algorithm is exact for the particle within the cutoff and is dominated by the inherent errors on the mesh. In the present case, the errors are of the order of 30%, 10%, and 5%, for $r_c/h = 1$, 2 and 3, respectively.

A second test case involves 10^4 charged particles uniformly distributed at the center of the domain, and we consider the error of the force on a test particle at different distance from the group (see Fig. 12b). For this case, the maximum error is of the order of 2% for $r_c/h = 3$.

5. Summary and conclusions

We have presented molecular dynamics simulations of the hydrophobic/hydrophilic nature of carbon nanotubes in water. Using a detailed description of the carbon nanotube and classical potentials for the carbon-water interaction including an electrostatic quadrupole moment acting between the carbon atoms and the charge sites on the water, we find structural properties of water similar to those found for water at a idealized graphite surface. However, in the present case, the water is slightly inclined with an angle of $\approx 4^\circ$ at the interface with a preferred orientation of the water dipole moment and OH bonds pointing towards the carbon nanotube. The quadrupole moment has a negligible contribution to the density and water dipole moment, but it appears to intensify the probability distribution of the orientation of the OH bonds. Further studies are being conducted to confirm these results.

Molecular dynamics simulations of two carbon nanotubes in water have revealed a continuous "wetting" or a "drying" of the interstice between the tubes depending on their initial spacing. For the present carbon nanotubes with a chirality of $(16, 0)$ (diameter of 12.52 Å), tube spacings of 7 and 8 Å resulted in a drying of the interstice whereas an initial spacing of 9 Å resulted in a permanent wetting. These results are in agreement with earlier studies of stacked plates by Wallqvist & Berne (1995) which indicate that stable configurations of water in a hydrophobic environment require the presence of two or more water layers. We are currently in the process of analyzing these results to determine the driving mechanisms of the drying process.

Acknowledgments

We wish to acknowledge discussions with Andrew Pohorille, Michael Wilson, and Michael New at NASA Ames Computational Astrobiology Branch, and with Flavio Noca from the Jet Propulsion Laboratory.

REFERENCES

Allen, M. P. & Tildesley, D. J. 1987 *Computer Simulation of Liquids.* Clarendon Press Oxford.

Allen, T. W., Kuyucak, S. & Chung, S.-H. 1999 The effect of hydrophobic and hydrophilic channel walls on the structure and diffusion of water and ions. *J. Chem. Phys.* **111** (17), 7985-7999.

Andrea, T. A., Swope, W. C. & Andersen, H. C. 1984 The role of long ranged forces in determining the structure and properties of liquid water. *J. Chem. Phys.* **79** (9), 4576-4584.

Balavoine, F., Schultz, P., Richard, C., Mallouh, V., Ebbesen, T. W. & Mioskowski, C. 1999 Helical crystallization of proteins on carbon nanotubes: A first step towards the development of new biosensors. *Angew. Chem.* **38** (13/14), 1912-1915.

Becke, A. D. 1993 Density-functional thermochemistry. III. the role of exact exchange. *J. Chem. Phys.* **98**, 5648-5652.

Dang, L. X. & Pettitt, M. 1987 Simple intramolecular model potentials for water. *J. Phys. Chem.* **91**, 3349-3354.

Frisch, M. J., *et al.* 1998 *Gaussian 98*, revision a.7. Tech. Rep. Gaussian, Inc., Pittsburgh PA.

Gordon, P. A. & Saeger, R. B. 1999 Molecular modeling of adsorptive energy storage: Hydrogen storage in single-walled carbon nanotubes. *Ind. Eng. Chem. Res.* **38**, 4647-4655.

Guo, Y., Karasawa, N. & Goddard III, W. A. 1991 Prediction of fullerene packing in C_{60} and C_{70} crystals. *Nature.* **351**, 464-467.

Hansen, F. Y. & Bruch, L. W. 1995 Molecular-dynamics study of the dynamical excitations in commensurate monolayer films of nitrogen molecules on graphite: A test of the corrugation in the nitrogen-graphite potential. *Phys. Rev. B.* **51** (4), 2515-2536.

Hockney, R. W. & Eastwood, J. W. 1988 *Computer Simulation Using Particles*, 2nd edn. IOP.

Jarvis, S. P., Uchihashi, T., Ishida, T. & Tokumoto, H. 2000 Local solvation shell measurement in water using a carbon nanotube probe. *J. Phys. Chem. B.* **104** (26), 6091-6094.

Lee, C. Y., McCammon, J. A. & Rossky, P. J. 1984 The structure of liquid water at an extended hydrophobic surface. *J. Chem. Phys.* **80** (9), 4448-4455.

Lee, S. M. & Lee, Y. H. 2000 Hydrogen storage in single-walled carbon nanotubes. *Appl. Phys. Lett.* **76** (20), 2877-2879.

Levitt, M., Hirshberg, M., Laidig, K. E. & Daggett, V. 1997 Calibration and testing of a water model for simulation of the molecular dynamics of proteins and nucleic acids in solution. *J. Phys. Chem. B* **101**, 5051-5061.

Li, J., Cassell, A. M. & Dai, H. 1999 Carbon nanotubes as AFM tips: Measuring DNA molecules at the liquid/solid interface. *Surface and Interface Analysis.* **28**, 8-11.

Lum, K., Chandler, D. & Weeks, J. D. 1999 Hydrophobicity at small and large length scales. *J. Phys. Chem. B* **103**, 4570-4577.

Marković, N., Andersson, P. U., Någård, M. B. & Petterson, J. B. C. 1999 Scattering of water from graphite: simulations and experiments. *Chem. Phys.* **247**, 413-430.

Marković, N., Andersson, P. U., Någård, M. B. & Petterson, J. B. C. 2000 Erratum to "scattering of water from graphite: simulations and experiments" [Chem. Phys. **247** (1999) 413-430). *Chem. Phys.* **252**, 409-410.

Mizan, T. I., Savage, P. E. & Ziff, R. M. 1994 Molecular dynamics of supercritical water using a flexible SPC model. *J. Phys. Chem.* **98**, 13067-13076.

Moloni, K., Buss, M. R. & Andres, R. P. 1999 Tapping mode scaling force microscopy in water using a carbon nanotube probe. *Ultramicroscopy.* **80**, 237-246.

Müller, E. A., Rull, L. F., Vega, L. F. & Gubbins, K. E. 1996 Adsorption of water on activated carbons: A molecular simulation study. *J. Phys. Chem.* **100** (4), 1189-1196.

Odom, T. W., Huang, J.-L., Kim, P. & Lieber, C. M. 2000 Structure and electronic properties of carbon nanotubes. *J. Phys. Chem. B.* **104**, 2794-2809.

Rappé, A. K., Casewit, C. J., Colwell, K. S., Goddard III, W. A. & Skiff, W. M. 1992 UFF, a full periodic table force field for molecular mechanics and molecular dynamics simulations. *J. Am. Chem. Soc.* **114**, 10024-10035.

Rzepka, M., Lamp, P. & de la Casa-Lillo, M. A. 1998 Physisorption of hydrogen on microporous carbon and carbon nanotubes. *J. Phys. Chem. B.* **102**, 10894-10898.

Saito, R., Takeya, T., Kimura, T., Dresselhaus, G. & Dresselhaus, M. S. 1998 Raman intensity of single-wall carbon nanotubes. *Phys. Rev. B.* **57** (7), 4145-4153.

Shevade, A. V., Jiang, S. & Gubbins, K. E. 1999 Adsorption of water-methanol mixtures in carbon and alumino-silicate poares: a molecuar simulation study. *Mol. Phys.* **97** (10), 1139-1148.

Teleman, O., Jönsson, B. & Engström, S. 1987 A molecular dynamics simulation of a water model with intramolecular degrees of freedom. *Mol. Phys.* **60** (1), 193-203.

Theuns, T. 1994 Parallel P3M with exact calculation of short range forces. *Comp. Phys. Commun.* **78**, 238-246.

Tuzun, R. E., Noid, D. W., Sumpter, B. G. & Merkle, R. C. 1996 Dynamics of fluid flow inside carbon nanotubes. *Nanotech.* **7** (3), 241-248.

Ulberg, D. & Gubbins, K. E. 1995 Water adsorption in microporous graphite carbons. *Mol. Phys.* **84** (6), 1139-1153.

Vernov, A. & Steele, W. A. 1992 The electrostatic field at a graphite surface and its effect on molecule-solid interactions. *Langmuir.* **8**, 155-159.

Wallqvist, A. 1990 Polarizable water at a hydrophobic wall. *Chem. Phys. Lett.* **165** (5), 437-442.

Wallqvist, A. & Berne, B. J. 1995 Computer simulation of hydrophobic hydration forces on stacked plates at short range. *J. Phys. Chem.* **99**, 2893-2899.

Wallqvist, A. & Teleman, O. 1991 Properties of flexible water models. *Mol. Phys.* **74** (3), 515-533.

Walther, J. H. & Koumoutsakos, P. 2000 An influence matrix P^3M algorithm with exact particle-particle correction. *In preparation* .

Wang, Q. & Johnson, J. K. 1999 Optimization of carbon nanotubes arrays for hydrogen adsorption. *J. Phys. Chem. B.* **103**, 4809-4813.

Whitehouse, D. B. & Buckingham, A. D. 1993 Experimental determination of the atomic quadrupole moment of graphite. *J. Chem. Soc. Faraday Trans.* **89** (12), 1909-1913.